Available online at www.sciencedirect.com

ScienceDirect

Procedia Engineering 102 (2015) 1356 – 1365

Procedia Engineering

www.elsevier.com/locate/procedia

The 7th World Congress on Particle Technology (WCPT7)

A meso-scale model for fluid-microstructure interactions

Rodrigo Guadarrama-Lara*, Xiaodong Jia, Michael Fairweather

Institute of Particle Science and Engineering, School of Process, Environmental and Materials Engineering, University of Leeds, Leeds LS2 9JT, UK

Abstract

Particle-fluid and fluid-structure interactions are important areas in particle technology. Typical processes where such interactions are prevalent include fluidized beds, filtration and sedimentation. In addition, fluid-structure interactions are significant in applications such as nuclear waste management, for example in the cementation process used to store radioactive materials, as well as in carbon capture and storage applications where the leakage of gas injected in underground geological reservoirs must be considered in hazard and risk assessments. Given the difficulties in directly measuring the propagation of cracks in solid structures, their permeability or the internal build-up of any gases, for example, numerical techniques in conjunction with non-destructive measurements are important tools of value in assessing and predicting the behavior of fluid-structure interactions. In this work, coupling between the lattice Boltzmann method and a digital packing algorithm based on the discrete element method is used to provide a basis for predicting such coupled interactions. The development of the coupled algorithm is described, with the calculations performed on a regular lattice grid and based on the momentum exchange method to evaluate the force exerted by the fluid on a solid boundary. A number of test cases are reported to allow assessment of the coupled model's capabilities. Overall, these test cases demonstrate reasonable quantitative agreement with available analytical and experimental results for the case of a sphere settling in a liquid, and the expected qualitative behavior for the case of different orientation cylinders settling in a fluid, and for three dynamic packing processes.

Selection and peer-review under responsibility of Chinese Society of Particuology, Institute of Process Engineering, Chinese Academy of Sciences (CAS)

Keywords: Fluid-structure interaction; Lattice Boltzmann method; Discrete element method; Complex structures.

* Corresponding author. Tel.: +44-113-343-2350; fax: +44-113-343-2384.
E-mail address: pmrgl@leeds.ac.uk

Selection and peer-review under responsibility of Chinese Society of Particuology, Institute of Process Engineering, Chinese Academy of Sciences (CAS)
doi:10.1016/j.proeng.2015.01.267

1. Introduction

The correct representation of real phenomena by computational programs is an area of active research and one which has direct relevance to many industrial applications. The available tools for performing such simulations must be accurate and efficient in order to provide reliable results. This is the case in many disciplines, including chemical and petroleum engineering, the pharmaceutical sciences, and earth and the environment, amongst others, where prediction of the potential behaviour of a particular system is necessary in cases where in situ experiments are expensive and difficult to carry out.

To understand the macroscopic behavior of particulate matter it is essential to examine microscopic inter-particle interactions, whether at the particle-particle or particle-fluid level, in order to correctly model systems and permit their interpretation through the use of predictive techniques. One relevant phenomenon is fluid-structure interaction (FSI) in which accurate simulation implies the construction of a methodology combining a solver for the Newtonian dynamics of the solid particles with a computational fluid dynamic (CFD) solver for the fluid. Those selected by the authors, and considered in this paper, are the discrete element method (DEM) together with the lattice Boltzmann method (LBM). LBM in particular has been used in recent years as an alternative approach to the conventional solution of the Navier-Stokes equations in computational fluid dynamic approaches, and has been demonstrated to be an efficient tool which is easy to implement in a computational code for performing simulations of fluid dynamic and FSI problems. A short review of FSI systems is considered below.

In chemistry, the behavior and properties of emulsions, suspensions and cakes can be predicted when flocculants are present or absent. Work in this area has been undertaken [1] to couple DEM and CFD to simulate particle filtration and cake formation, comparing the results obtained from simulations with experimental data. In the environmental sciences and civil engineering [2], leakage on the top side of an underground horizontal pipe has been assessed using a coupled DEM-LBM approach together with an immersed boundary scheme to simulate and predict the behavior of a cavity formed around the leak in two dimensions. Powder tableting processes used in the pharmaceutical industry are important in determining the quality of the final product for drug delivery, as considered in [3] using a finite-DEM approach, with wet and dry granulation versus a direct tableting mixture considered in [4]. Other applications can be found of relevance to nuclear waste processing; in [5] the authors present a study of the pore network in solid cemented structures to estimate the transport porosity by means of physical experiments, comparing the results of tritiated water diffusion with a proposed model, with the work presented in [6] making use of a coupled DEM-LBM technique to calculate the permeability in loose granular beds. The inter-particle interaction of nuclear fuel pebbles in a reactor was also assessed in [7] using DEM.

Much of the work performed to date has considered spherical particles. Extension of this research to encompass non-spherical particles can be made through the use of cutting edge tools that are also utilized to aid the representation of solids in computational simulations. The use of computed tomography (CT) and x-ray microtomography (XMT) is therefore acknowledged as a very useful approach for the x-ray imaging of the human body or any other objects and structures to assist in the analysis and study of materials, the internal structure of particles, and the understanding of related phenomena [8-10]. Complex porous networks can be generated using DEM or Monte Carlo techniques and the resulting structures from packing simulations can be used as input data for LBM simulations. However, and in the particular case of Monte Carlo-based algorithms, one of the disadvantages of this approach is that the dynamic packing process is considered to lack accuracy since the addition of particles and their arrangement is based on assumptions about particle motion and geometry. An attractive alternative is the use of CT images in LBM simulations for fluid transport and permeability predictions in porous media [11, 12].

2. Simulation and experimental techniques

2.1. Discrete element method

Numerical methods based on DEM treat the problem as a discrete system represented by a collection of independent particles in a domain. The formulation of such methods finds its fundamentals in algorithms tracking the contacts between particles, their kinematics and deformations (if present); the objective is the modelling of a physical dynamic process accounting for the multi-contact points and the displacements produced by the particle

interactions. The effective implementation of DEM has proved to be an attractive numerical simulation tool. Since the early developments in the 1970's [13, 14], the analysis of granular materials made up of discrete particles through DEM has allowed a more realistic interpretation of material behavior due to the explicit way in which particle interactions at their contact points are accommodated. A great number of researchers have found the technique useful, and have developed modifications and improvements along with ever improving computational capabilities [15, 16], allowing the interaction of ever larger numbers of complex shapes to be predicted.

In DEM, all the forces acting on a particle in a particular system originate from the interaction with neighboring particles, from physical boundaries and from external forces. If such forces are known, then the computation is reduced to the integration of Newton's equation of motion:

$$\vec{f}_i = m_i \cdot \dot{a} = \frac{d^2\vec{x}_i}{dt^2} \tag{1}$$

where $\vec{f}_i$ is the total contact force as a result of the addition of all the forces acting on the particle, m_i is the mass of the i^{th} particle and $\vec{a}$ is the corresponding acceleration which is equal to the second derivative of the particle position x_i. The modelling process takes the form of an iterative cycle by first detecting the contact points on every particle at a given time, with the forces applied on such points calculated based on the known velocity of the colliding particle. The sum of all the forces on the particles then allows the new accelerations of the particles to be determined, and hence their corresponding velocities, which are then used to update the particle positions by numerical integration over a small time step. Once the new velocities and positions are found for each particle, the cycle starts again by detecting particle contacts and computing the respective forces.

2.2. Lattice Boltzmann method

LBM is a numerical method based on the microscopic representation of a fluid by a particle distribution function (PDF), discretized in space and time. It evolved from the lattice gas cellular automata approach [17, 18] and is considered an alternative to traditional CFD methods based on direct solution of the Navier-Stokes equations. In its most general form, physical space or the domain of interest is represented by a regular lattice which allocates particles at discrete nodes; the particles are then allowed to move from one node to a neighboring node and may collide with other particles located at those nodes. Since the methodology aims to represent the physics of a real system, the lattice grid where the PDF lies should be sufficiently resolved and the time step small enough to ensure simulation accuracy and stability, and in order to recover the continuum parameters such as density and fluid velocity of the macroscopic system.

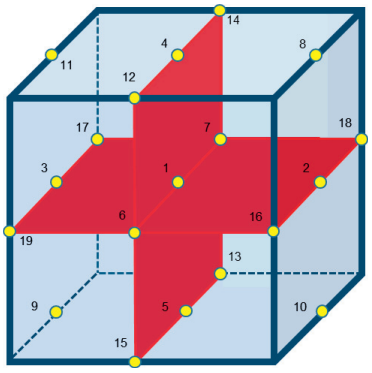

Fig. 1. Velocity vectors in the D3Q19 model.

The grid considered in the present work is a three-dimensional mesh in which every lattice node is given by a basic unit of lattice spacing of length $\delta_x=1$; the time step is set as $\delta_t=1$and the speed is given in terms of the non-

dimensional speed of sound c_s, defined as $c_s=c/\sqrt{3}$ where $c=\delta_x/\delta_t$. The Boltzmann model reduces the possible particle positions and momenta to a few confined nodes in the lattice in the discretized time. In the D3Q19 model shown in Figure 1, the particle may remain at rest at position 1 (centre) or move according to one of the eighteen possible different velocity vectors e_i (numbers 2 to 19).

The PDF $f(x, e_i, t)$ is defined as the number of particles at time t that are located in position x with a particular velocity e_i, with the subscript i being one of the 19 discrete velocities. In the discretized Boltzmann equation [19], the time dependent movement of the particles at each node satisfies the expression:

$$f_i\left(x+e_i,t+\Delta t\right)=f_i\left(x,t\right)-\frac{1}{\tau}\left[f_i\left(x,t\right)-f_i^{eq}\left(x,t\right)\right] \tag{2}$$

The relaxation time τ in Eq. (2) is related to the viscosity of the fluid according to $\tau=3v+0.5$. LBM consists of two steps which correspond to propagation and collision. The propagation or streaming step (Eq. (3)) moves the PDF to the adjacent cell according to the velocity vector:

$$f_i\left(x,t+\Delta t\right)=f_i\left(x+e_i,t\right) \tag{3}$$

The second term on the right-hand side of Eq. (2) describes the collision operator in which all the distribution functions relax at a single rate to the equilibrium values. For the D3Q19 model used, the equilibrium distribution function f_i^{eq} is given by Eq. (4):

$$f_i^{eq}\left(x\right)=\omega_i\rho\left[1+\frac{e_i\cdot u}{c_s^2}+\frac{\left(e_i\cdot u\right)^2}{2c_s^4}-\frac{u^2}{2c_s^2}\right] \tag{4}$$

The ω_i in this expression are constant weighting factors related to the velocity vectors [20]. The macroscopic variables of the fluid density ρ and velocity $\boldsymbol{v}$ are recovered from the moments of the fluid PDF as follows:

$$\rho=\sum_{1}^{19}f_i \tag{5}$$

$$\vec{v}=\frac{1}{\rho}\sum_{1}^{19}f_i e_i \tag{6}$$

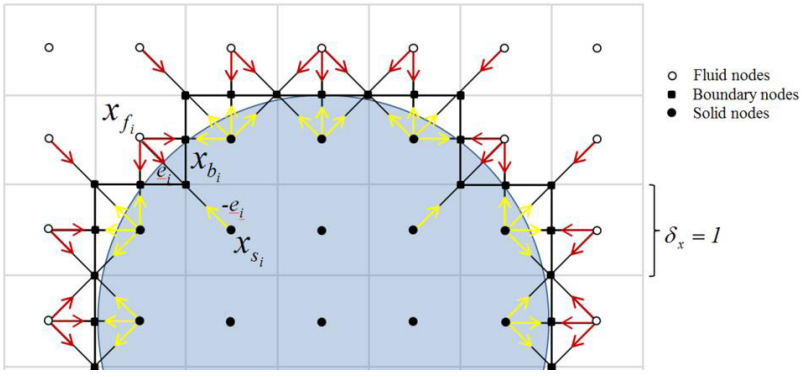

Fig. 2. Representation of a half of a sphere in a lattice domain.

The density of the fluid is considered constant in the lattice domain and equally distributed in the velocity field. As can be observed in Figure 2, the lattice nodes may be solid nodes (solid circles) and fluid nodes (open circles). The links between one fluid node x_{fi} and one solid node x_{si} yields a boundary node x_{bi} located between the two (solid squares). For further details of the basis of the technique, and its application, the reader is referred to [21-25].

2.3. Solid-fluid boundary considerations

In the model considered, it is necessary to incorporate the boundary conditions that the solid imposes on the fluid nodes. As shown previously in Figure 2, the fluid-structure interaction takes place in the boundary nodes formed by the fluid-solid node links. The no-slip, bounce-back boundary condition is implemented by ensuring that the fluid nodes adjacent to the boundary nodes are reflected or 'bounced-back' to the same fluid node, thus, the bounce velocity is the same as that before collision but in the opposite direction [26]. In order to advance in the subsequent propagation step, the momentum of an incoming fluid node is bounced-back in the opposite direction, $-e_i$, to the static boundary node; this is represented in Eq. (7) where $\tilde{f}$ is a post-collision PDF:

$$\tilde{f}_{-i}\left(x,t+1\right)=\tilde{f}_{i}\left(x,t\right) \tag{7}$$

2.4. X-ray microtomography

The XMT technique used in the present work to obtain digitized images of complex geometry particles such as sand grains is a methodology based on the acquisition of a large number of images (hundreds or thousands depending on the targeted image detail) in two dimensions which are subsequently used to construct a three-dimensional representation by stacking the two-dimensional images together. Once the total volume is reconstructed, a post-processing stage is used to enhance the visualization of the structure, or to focus on specific elements of interest. Practically any sample of any shape, within the maximum size constraints of the equipment used, can be placed in the scanner; for instance, one may obtain digitized images by scanning an individual particle and using it to make up a packed bed, or by scanning a packed bed made up of different particles and using it directly in LBM for fluid flow simulations in structures made of different materials such as sand, soil, rocks, powder, etc. If desired, segmentation can be achieved with the appropriate post-processing software for the extraction of individual particle details which can be used as the basis, for example, of simulations of the dynamic packing process using DEM. The inherent advantage of this technique is that the digital image embeds the shape, surface texture and internal structure of both regular and complex geometries.

3. DEM and LBM software validation

The in-house software that served as a starting point for the coupled algorithm implementation is called DigiPac [27] which is made up of a number of different modules, two of them relevant for the coupling work described herein, namely DigiDEM and DigiFlow (based on LBM). DigiPac also contains a module that can be used for the post-processing of XMT images. As an initial step both elements of this software were validated separately, first for packing simulations (using DEM) and secondly for simulations of fluid flow through porous structures (LBM) to assess their accuracy. Packed structures were generated using glass spheres, with the various packing configurations considered outlined in Table 1.

Table 1. Sphere packing configurations.

	Case A	Case B	Case C
Sphere diameter / mm	2	1	0.3
Cylindrical container diameter / mm	10	10	10
Particle to container size ratio	0.2	0.1	0.03

Additionally, two more beds were generated using sand grains, one with a mean grain size of 250 µm and another of 300 µm. All five packings were imaged using XMT to obtain digital three-dimensional representations of the beds. Segmentation was carried out on the sand structures in order to obtain individual sand grain details for use in the packing process simulations; for packing spheres, one single packing was digitally created using a different module in DigiPac according to the specifications shown in Table 1. In Figure 3, by way of illustration of results typical of those obtained for all cases, a comparison of experimental and simulation results for sphere Case B and the sand bed made up of 300 µm particles are presented. These packing profiles demonstrate that the simulations closely follow the experimental observations. Using these results, derived porosities were larger in the simulations for all five cases with, for example, Case B exhibiting a maximum error of 11.2% relative to the XMT reference porosity.

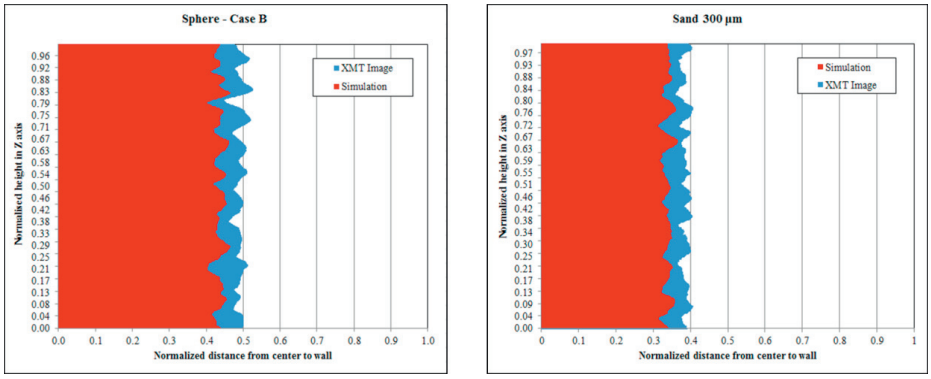

Fig. 3. Central region packing profile for sphere Case B (left) and 300 µm sand grains (right).

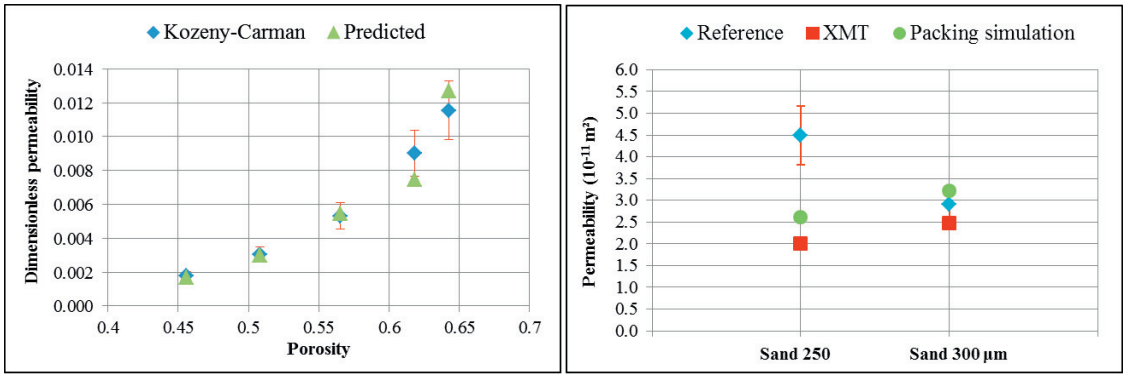

Fig. 4. Comparison of permeability predictions obtained using LBM with analytical and experimental results.

For the lattice Boltzmann simulations, predicted permeability values were compared with theoretical values obtained using the Kozeny-Carman equation [28] for the case of a bed made up of mono-sized spheres. For a range of porosities the left hand side of Figure 4 shows good agreement between these two predictive approaches, with LBM results following the analytical values (with error bars of 15% shown for the latter). The sand beds noted above were also used for validation purposes, with XMT scans used as input data for the fluid flow simulations. In this case, experimental data found in the literature [29] were used as the basis for comparison with predicted permeabilities, the results of which are shown on the right hand side of figure 4 (with 15% error bars shown for the reference data). Again, acceptable agreement was found for these more complex packing cases.

4. Coupled code implementation and test cases

For implementation of the coupled code a partitioned method was selected due to the nature of DigiPac, i.e. the solver for the fluid domain is separate from that for the solid domain. The corresponding equations were therefore solved internally in the code; first the fluid calculation was performed to evaluate the stress exerted on the solid walls, with the results then used to update the positions of the solid. Having updated the boundary wall positions an iterative process continued until convergence.

4.1. Code implementation

To evaluate the force exerted on the solid boundary by the fluid two different approaches are available; one is known as the stress integration method [26] and the second is the momentum exchange method [30]. In the first, the force on a body is evaluated by integrating the total stresses on its surface; in the latter, the forces centrally located between the fluid and solid node links are calculated from the momentum exchange as the summation of all the forces from neighboring fluid nodes applied on a solid boundary node, as shown in Figure 2. For example, one incoming forces x_f is acting on x_s. The total force applied on the particle is then given by the summation of all the incoming forces on all the solid boundary nodes x_b.

Within the LBM simulation the following actions were performed in sequence: streaming, bounce-back, collision (updating $f = f + f^{eq}$) and the force calculation. The force scaling factor $f_{scaling}$ used was:

$$f_{scaling} = f_{LB}\left(\frac{\nu_{ph}^2 \cdot \rho_{ph}}{\nu_{LB}^2 \cdot \rho_{LB}}\right)[N] \tag{8}$$

In Eq. (8), f is the force, ν is the kinematic viscosity in $m^2\ s^{-1}$ and ρ the density in kg m^{-3}. The subscripts *LB* and *ph* refer to the variables in the corresponding LBM system and the real physical system, respectively. For the simulations, the relaxation time was set to 1, therefore the viscosity in the system is $\nu = 1/6$ and the density of the fluid is deemed to be uniform and hence equal to 1. The force exerted by the fluid on a particle was calculated using the momentum exchange algorithm introduced by Ladd [30]. As presented above, the resultant total force is obtained by summation over the entire fluid-solid boundary links, with the force calculated following [31]:

$$F_i'\left(x+\frac{1}{2}e_i\Delta t, t+\frac{1}{2}\Delta t\right) = \left[f_i\left(x,t^+\right) - f_i'\left(x+e_i\Delta t, t^+\right) - 2\omega_i\rho v_b \cdot e_i\right]e_i \tag{9}$$

where v_b is the boundary velocity given by:

$$v_b = U_p + \Omega_p \times \left[\left(x+\frac{1}{2}e_i\Delta t\right) - X_p\right] \tag{10}$$

Here, U_p is the translational velocity, Ω_p the rotational velocity and X_p the centroid of the particle. Once the LBM force is calculated, it is then passed to the DEM to perform the corresponding calculations, as noted above.

4.2. Test cases

To validate the coupled code implementation a number of test cases were performed. The first case simulated was the flow past a single sphere. For this case, the analytical drag forces, F_d, from the Stokes and Rayleigh equations can be compared with values computed in the simulations. Different configurations were examined by modifying the sphere diameter and its settling velocity in the fluid, but below only the results obtained for the case of a sphere with diameter of 20 pixels (equivalent to 0.02 m) are presented for the sake of brevity. The simulation

domain was 0.12×0.12×0.5 m, with these being the width, depth and height (z axis) of the system, respectively. The fluid flow calculation used a constant body force to simulate the pressure difference in the system, with the fluid flowing upwards and passing the sphere which was placed in the geometrical centre of the system. Additionally, for the Reynolds numbers, Re, considered, which ranged from 0.25 to 260, the calculated drag coefficient, C_d, was compared with the equation presented in [32].

Three more simulations were performed to similarly assess the behavior of a cylinder of length to diameter ratio of 4 settling in a fluid, with the cylinder first released in a vertical position, then in a horizontal position, and finally with an initial inclination of 45°. The numerical solution domain used was 0.128×0.128×0.500 m, with the top and bottom boundaries set as periodic to allow the cylinder to continue fall beyond the z axis length of 0.5 m.

Lastly, three dynamic packing processes were simulated, using selected three-dimensional digitized images of sand grains previously obtained at the validation stage, which were used to qualitatively compare the resulting packed structures. The sand grains were added to a domain of 0.36×0.36×0.80 m for three different configurations; settling in a vacuum, settling in LBM fluid, and settling in a Stokes plug flow.

5. Results and conclusions

Results obtained from the first test case of a settling sphere are presented in Figure 5. On the left hand side analytical values of the drag force are shown against the present predictions. For Re < 260, the simulations are in good agreement with analytical values from the Rayleigh equation, after which point the simulations tend to follow the Stokes equation values, but deviate from them by up to a factor of 4.3. On the right hand side of this figure, the corresponding drag coefficients are presented and compared with the expression of Morrison [32], with good agreement found.

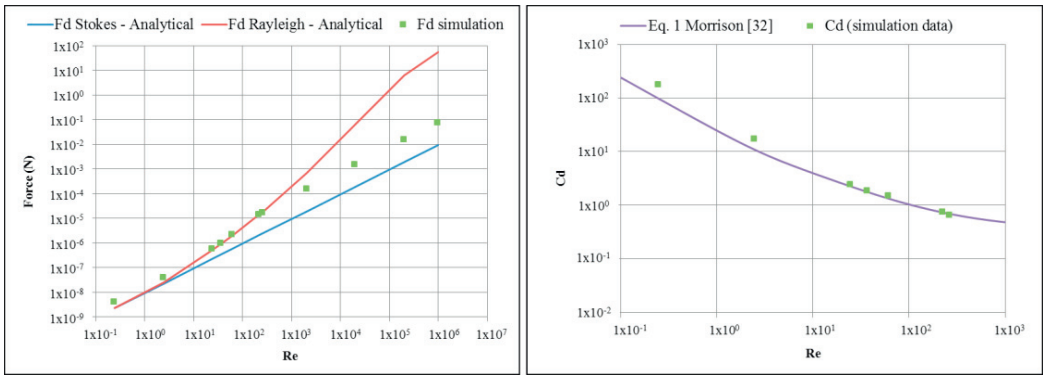

Fig. 5. Comparison of predicted drag force and drag coefficient with analytical and experimental values.

The results obtained for the second test case demonstrated that when the cylinder settles from an initially horizontal or vertical position the same qualitative behavior is observed. Hence, for such initial conditions it is expected that the fluid exerts the same drag force on the surface of the cylinder, and thus the force vectors pushing the cylinder upwards are balanced over the surface area and the object does not tumble. In contrast, for the case where the cylinder was initially placed in a tilted position, it is observed that it eventually turns due to the presence of the expected torque force. The evolution of this last case is illustrated in Figure 6.

Lastly, Figure 7 shows the early stages of the simulation of the three dynamic packing processes. The particles were added in groups of ten, and it can be observed that in a vacuum there are two layers of particles which show neither rotation nor translation while settling. When settling in LBM fluid and plug flow, however, the effect of the fluid acting on the surface of the particles can be observed as it exerts an upward force on them, delaying their settling. Once settled, the packing fraction profile along the normalized z axis for the three different simulations was also assessed. To minimize wall effects, this was done by considering the central region of every packed structure, which allowed calculated porosities of 0.417, 0.436 and 0.440 for the simulations in a vacuum, in a fluid and in plug

flow to be derived. Although these three values correspond to structures packed under different conditions, the resulting almost constant porosity is consistent with the expected behavior.

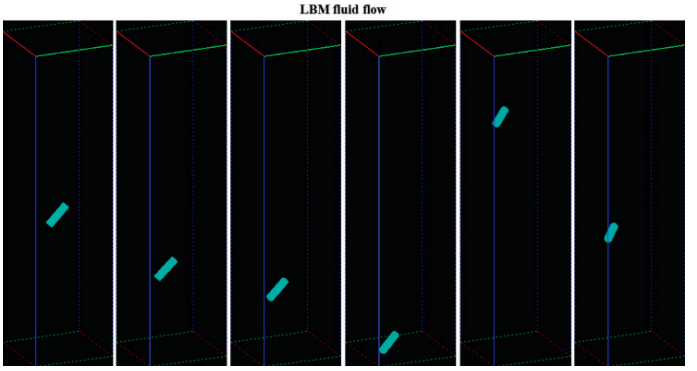

Fig. 6. Cylinder settling in a fluid flow (time advancing left to right, where top and bottom boundaries are periodic).

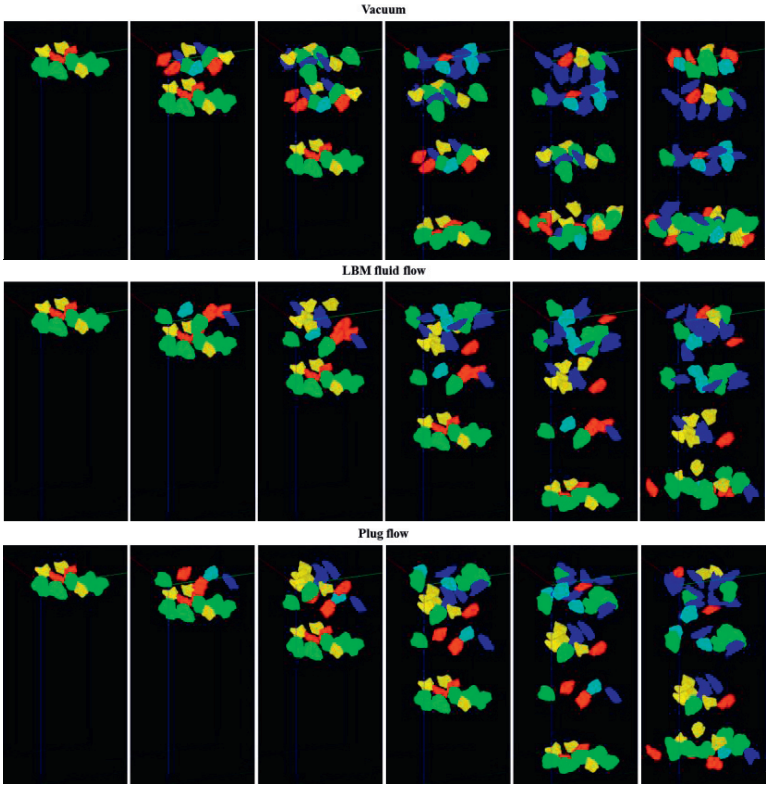

Fig. 7. Settling particles in the three dynamic packing process simulations.

Overall, the numerical test cases considered show reasonable quantitative agreement with available analytical and experimental results for the settling sphere case, and the expected qualitative behavior for the case of different orientation cylinders settling in a fluid, and for the three dynamic packing processes examined. Future work will focus on further quantitative validation of the coupled modelling approach through application to some of the practically important cases mentioned in the introduction.

References

[1] S. Stein, J. Tomas, Modelling of the filtration behavior using coupled DEM and CFD, in: C.-Y. Wu, Discrete Element Modelling of Particulate Media, The Royal Society of Chemistry, 2012, pp. 113-120.

[2] X. Cui, J. Li, A.H.C. Chan, D. Chapman, The effect of initial bed height on the behavior of a soil bed due to pipe leakage using the coupled DEM-LBM technique, in: C.-Y. Wu, Discrete Element Modelling of Particulate Media, The Royal Society of Chemistry, 2012, pp. 51-58.

[3] R.W. Lewis, D.T. Gethin, X.S. Yang, R.C. Rowe, A combined finite-discrete element method for simulating pharmaceutical powder tableting, Int. J. Numer. Meth. Engng. 62 (2005) 853-869.

[4] M. Šantl, I. Ilić, F. Vrečer, S. Baumgartner, A compressibility and compactibility study of real tableting mixtures: The impact of wet and dry granulation versus a direct tableting mixture, Int. J. Pharm. 414 (2011) 131-139.

[5] T. Yamaguchi, K. Negishi, S. Hoshino, T. Tanaka, Modelling of diffusive mass transport in micropores in cement based materials, Cement Concrete Res. 39 (2009) 1149-1155.

[6] M. Mansouri, J.-Y. Delenne, A. Seridi, M.S. El Yossoufi, Numerical model for the computation of permeability of a cemented granular material, Powder Technol. 208 (2011) 532-536.

[7] H. Suikkanen, J. Ritvanen, P. Jalali, R. Kyrki-Rajamäki, Modeling packing of spherical fuel elements in pebble bed reactors using DEM, in: C.-Y. Wu, Discrete Element Modelling of Particulate Media, The Royal Society of Chemistry, 2012, pp. 175-183.

[8] M. Suzuki, T. Shinmura, K. Iimura, M. Hirota, Study of the wall effect in particle packing structure using x-ray micro computed tomography, Adv. Powder Technol. 19 (2008) 183-195.

[9] A.R. Videla, C.L. Lin, J.D. Miller, 3D characterization of individual multiphase particles in packed particle beds by x-ray microtomography (XMT), Int. J. Miner. Process. 84 (2007) 321-326.

[10] J.M. Schembre, A.R. Kovscek, A technique for measuring two-phase relative permeability in porous media via x-ray CT measurements, J. Petrol. Sci. Eng. 39 (2003) 159-174.

[11] M.S. Islam, R. Caulkin, X. Jia, M. Fairweather, R.A. Williams, Prediction of the permeability of packed beds of non-spherical particles, Computer Aided Chemical Engineering 30 (2012) 1088-1092.

[12] C.L. Lin, A.R. Videla, J.D. Miller, Advanced three-dimensional multiphase flow simulation in porous media reconstructed from X-ray Microtomography using the He-Chen-Zhang Lattice Boltzmann Model, Flow Meas. Instrum. 21 (2010) 255-261.

[13] P.A. Cundall, A computer model for simulating progressive large-scale movements in block rock mechanics, Proc. Symp. Int. Soc. Rock Mech., Nancy, p II-8.

[14] P.A. Cundall, O.D.L. Strack, A discrete numerical model for granular assemblies, Geotechnique 29 (1979) 47-65.

[15] H.P. Zhu, Z.Y. Zhou, R.Y. Yang, A.B. Yu, Discrete particle simulation of particulate systems: Theoretical developments, Chem. Eng. Sci. 62 (2007) 3378-3396.

[16] D. Zhao, E.G. Nezami, Y.M.A. Hashash, J. Ghaboussi, Three-dimensional discrete element simulation for granular materials, Eng. Computation. 23 (2006) 749-770.

[17] D. Rothman, S. Zaleski, Lattice-gas cellular automata: Simple models of complex hydrodynamics, Collection Alea Saclay, 1997, New York, U.S.A.

[18] G.R. McNamara, G. Zanetti, Use of the Boltzmann equation to simulate lattice-gas automata, Phys. Rev. Lett. 61 (1988) 2332-2335.

[19] R. Mei, D. Yu, W. Shyy, et.al., Force evaluation in the lattice Boltzmann method involving curved geometry, Phys. Rev. E. 65 (2002).

[20] A.S. Joshi, Morphology transitions in multilayer polymer melts due to hole growth and layer interactions, PhD dissertation, Graduate School of Clemson University, 2005.

[21] A.R. Videla, C.L. Lin, J.D. Miller, Simulation of saturated fluid flow in packed particle beds – The lattice-Boltzmann method for the calculation of permeability from XMT images, J. Chin. Inst. Chem. Eng. 39 (2008) 117-128.

[22] X. He, L-S. Luo, Lattice Boltzmann model for the incompressible Navier-Stokes equation, J. Stat. Phys. 88 (1997) 927-944.

[23] S. Chen, G.D. Doolen, Lattice Boltzmann method for fluid flows, Annu. Rev. Fluid Mech. 30 (1998) 329-364.

[24] D.A. Wolf-Gladrow, Lattice-gas cellular automata and lattice Boltzmann models – An introduction, Springer, 2005.

[25] S. Succi, The lattice Boltzmann equation for fluid dynamics and beyond, Oxford Science Publications, 2001.

[26] X. He, D. Doolen, Lattice Boltzmann method on curvilinear coordinates systems: Flow around a circular cylinder, J. Comput. Phys. 134 (1997) 306-315.

[27] X. Jia, R.A. Williams, A packing algorithm for particles of arbitrary shapes, Powder Technol. 120 (2001) 175-186.

[28] P. Xu, B. Yu, Developing a new form of permeability and Kozeny-Carman constant for homogeneous porous media by means of fractal geometry Adv. Water Resour. 31 (2008) 74-81.

[29] M. Huettel, W. Ziebis, S. Forster, Flow-induced uptake of particuate matter in permeable sediments, Limnol. Oceanogr. 41 (1996) 309-322.

[30] A.J.C. Ladd, Numerical simulations of particulate suspensions via a discretized Boltzmann equation Part 1. Theoretical foundation, J. Fluid Mech. 271 (1994) 285-309.

[31] D.R.J. Owen, C.R. Leonardi, Y.T. Feng, An efficient framework for fluid-structure interaction using the lattice Boltzmann method and immersed moving boundaries, Int. J. Numer. Meth. Engng. 87 (2011) 66-95.

[32] F.A. Morrison, Data correlation for drag coefficient for sphere, Department of Chemical Engineering, Michigan Technological University, 2013.